

Lattice Boltzmann Model for Free Surface Flow for Modeling Foaming

C. Körner,¹ M. Thies,¹ T. Hofmann,¹ N. Thürey,² and U. Rude²

Received October 12, 2004; accepted September 13, 2005

We present a 2D- and 3D-lattice Boltzmann model for the treatment of free surface flows including gas diffusion. Interface advection and related boundary conditions are based on the idea of the lattice Boltzmann equation. The fluid dynamic boundary conditions are approximated by using the mass and momentum fluxes across the interface, which do not require explicit calculation of gradients. A similar procedure is applied to fulfill the diffusion boundary condition. Simple verification tests demonstrate the correctness of the algorithms. 2D- and 3D-foam evolution examples demonstrate the potential of the method.

KEY WORDS: Lattice Boltzmann method; free surface flow; advection; diffusion; boundary conditions; foam.

1. INTRODUCTION

In many engineering areas, especially materials science, the dynamics of multiphase flow where one phase is a liquid and the other phase is a gas is important. Examples are all kind of casting methods, solidification of melts or – these are the processes we focus on – foaming processes.^(1,2,3) For many applications the dynamics of the gas can be neglected. That is, the two-phase flow problem can be reduced to a one-phase flow problem with free interfaces. Although the dynamics of the gas can be neglected gas diffusion within the melt combined with bubble nucleation and bubble growth is very often essential for the whole production process. This is not only true for foaming processes where blowing agents are deliberately

¹Materials Science and Technology WTM, University of Erlangen-Nueremberg, Martensstr. 5, 91058 Erlangen, Germany; e-mail: carolin.koerner@ww.uni-erlangen.de

²System Simulation Group, Cauerstr. 6, 91058 Erlangen, Germany.

added to the melt but also for normal casting processes where gas porosity develops during mould filling and subsequent solidification. In this paper the lattice Boltzmann method (LBM) is applied to flows with free gas–liquid interfaces where also gas diffusion is taken into account. We present formalisms for interface advection and the fulfillment of the boundary conditions within the LB formalism which are based on the kinetic interpretation of the LBM. Interface advection is realized with the help of a mass fraction variable, which is updated by recording the in- and outflow of mass via the distribution functions. For the reconstruction of the missing distribution functions at interface cells a current procedure is applied which provides exact control of the hydrodynamic momentum flux across the interface. A similar procedure is applied in order to match the diffusion boundary conditions. Surface tension effects and foam stabilization are included by adjusting the locally acting gas pressure.

2. BASIC EQUATIONS

The fundamental principle of the LBM is to solve the microscopic kinetic equation for particle distribution functions $f(\mathbf{x}, \boldsymbol{\xi}, t)$ where $(\mathbf{x}, \boldsymbol{\xi})$ are the phase space variables and t the time. It is well known that the particle velocity space $\boldsymbol{\xi}$ can be reduced to a small set of discrete velocities $\{\boldsymbol{\xi}_i | i = 1, \dots, b\}$ while preserving the hydrodynamic moments up to a certain order in $\boldsymbol{\xi}$.⁽⁴⁾ This discretization transforms the Boltzmann equation to a discrete equation. The lattice Boltzmann equation (LBE) follows from this discrete Boltzmann equation by an adequate space-time discretization,

$$f_i(\mathbf{x} + \mathbf{e}_i, t + 1) = f_i(\mathbf{x}, t) - \frac{1}{\tau} (f_i(\mathbf{x}, t) - f_i^{\text{eq}}(\mathbf{x}, t)) + F_i, \quad i = 0, 1, \dots, b, \quad (1)$$

where we use dimensionless lattice units and the dimensionless discrete velocity set $\{\mathbf{e}_i\}$, the relaxation time τ , the equilibrium distribution function of the i th discrete velocity $f_i^{\text{eq}}(\mathbf{x}, t) \equiv f_i^{\text{eq}}(\rho, \mathbf{v})$, the velocity \mathbf{v} , the density ρ and an external force (e.g., gravity) F_i . Equation (1) is based on the BGK-approximation where the collision term is treated by means of a single relaxation time approximation.⁽⁵⁾

For the fluid dynamic problem we use the two-dimensional D2Q9-model and the three-dimensional D3Q19-model.⁽⁶⁾ In this paper, diffusion is only implemented for the two-dimensional case where the D2Q4-model is employed.⁽⁷⁾ Figure 1 shows the respective velocity sets. The equilibrium distribution functions for the D2Q9- and D3Q19-models⁽⁶⁾ are defined as follows:

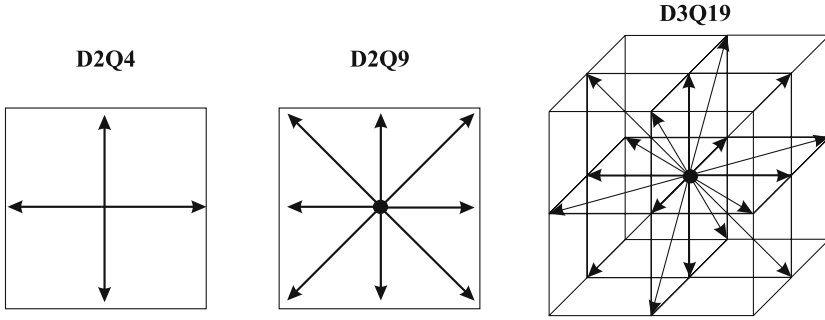


Fig. 1. Velocity sets for different LBMs: D2Q4, D2Q9 and D3Q19. Rest particles are defined in all models but the D2Q4.

$$f_i^{eq}(\rho, \mathbf{v}) = w_j \rho \left[1 + 3(\mathbf{e}_i \cdot \mathbf{v}) + \frac{9}{2}(\mathbf{e}_i \cdot \mathbf{v})^2 - \frac{3}{2}\mathbf{v} \cdot \mathbf{v} \right], \quad (2)$$

where $j = |\mathbf{e}_i|^2$ and $w_0 = \frac{16}{36}$, $w_1 = \frac{4}{36}$, $w_2 = \frac{1}{36}$ for the D2Q9-model and $w_0 = \frac{12}{36}$, $w_1 = \frac{2}{36}$, $w_2 = \frac{1}{36}$ for the D3Q19-model. Numerically, the LBE is solved in two steps, a streaming or advection step and a collision step:

Streaming $f_i^{in}(\mathbf{x}, t) = f_i^{out}(\mathbf{x} - \mathbf{e}_i, t - 1), \quad (3)$

Collision $f_i^{out}(\mathbf{x}, t) = f_i^{in}(\mathbf{x}, t) - \frac{1}{\tau} \left(f_i^{in}(\mathbf{x}, t) - f_i^{eq}(\mathbf{x}, t) \right) + F_i. \quad (4)$

During streaming (Equation (3)) all distribution functions but f_0 are advected to their neighbor lattice site defined by their velocity. After advection the particle distribution functions approach their equilibrium distributions due to a collision step (Equation (4)). The incoming and outgoing distribution functions, i.e., before and after collision, are denoted with f_i^{in} and f_i^{out} , respectively. The macroscopic density ρ and momentum $\rho \mathbf{v}$ in a cell are the 0th and 1th moments of the distribution functions,

$$\rho = \sum_{i=0}^b f_i, \quad \rho \mathbf{v} = \sum_{i=1}^b f_i \mathbf{e}_i. \quad (5)$$

The viscosity ν follows from: $\nu = \frac{1}{3}(\tau - \frac{1}{2})$.

The time evolution of the distribution functions g_i for the diffusion–convection problem is given by

$$g_i(\mathbf{x} + \mathbf{e}_i, t) = g_i(\mathbf{x}, t) - \frac{1}{\tau_D} (g_i(\mathbf{x}, t) - g_i^{\text{eq}}(\mathbf{x}, t)) + \frac{1}{4} Q \quad \text{for } i = 1, \dots, 4, \quad (6)$$

where τ_D is the relaxation time for diffusion and Q a source term. The equilibrium functions for the D2Q4-model are defined as follows:

$$g_i^{\text{eq}}(c, \mathbf{v}) = \frac{1}{4} c [1 + 3(\mathbf{e}_i \cdot \mathbf{v})] \quad \text{for } i = 1, \dots, 4, \quad (7)$$

where the velocity \mathbf{v} is given by $\mathbf{v} = \sum_i f_i \cdot \mathbf{e}_i / \sum_i f_i$. The concentration c follows from

$$c = \sum_{i=1}^4 g_i. \quad (8)$$

The diffusion constant D is given by $D = \frac{1}{2}(\tau_D - \frac{1}{2})$.

3. LBM FOR FREE INTERFACE

3.1. Free Surface and Fluid Advection

The description of the liquid–gas interface is very similar to that of volume of fluid methods. An additional variable, the volume fraction of fluid ϵ , defined as the portion of the area of the cell filled with fluid, is assigned to each interface cell. The representation of liquid–gas interfaces is depicted in Fig. 2.

Gas cells are separated from liquid cells by a layer of interface cells. These interface cells form a completely closed boundary in the sense that no distribution function is directly advected from fluid to gas cells and vice versa. This is a crucial point to assure mass conservation since mass coming from the liquid or mass transferred to the liquid always passes through the interface cells where the total mass is balanced. Hence, global conservation laws are fulfilled if mass and momentum conservation is ensured for interface cells. The cell types and their state variables and possible state transformations are listed in Table I. Per definition, the volume fraction ϵ of fluid and gas cells is 1 and 0, respectively. The fluid mass content of a cell is denoted with $M = M(\mathbf{x}, t)$. The mass content is a function of the volume fraction and the density. For a gas cell the fluid mass

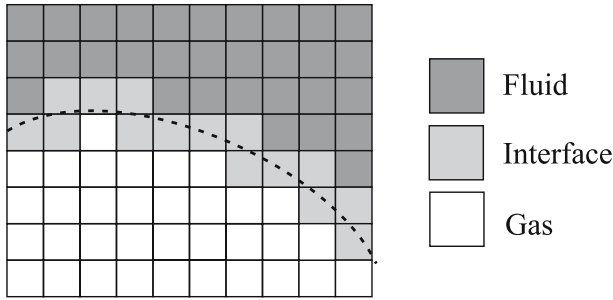


Fig. 2. 2D-Representation of a free liquid–gas interface by interface cells. The real interface (dashed line) is captured by assigning the interface cells their liquid fraction.

content M is zero whereas that of a fluid cell is given by its density ρ : $M(\mathbf{x}, t) = \rho(\mathbf{x}, t)$ for $\mathbf{x} \in F$, i.e., M and ρ are equivalent. Fluid cells gain and lose mass due to streaming of the f_i . If interface cells are considered, M and ρ are not equivalent and we have to account for the partially filled state by introducing a second parameter, the volume fraction $\epsilon = \epsilon(\mathbf{x}, t)$. The fluid mass content M , the volume fraction ϵ and the density ρ are related by $M(\mathbf{x}, t) = \rho(\mathbf{x}, t) \cdot \epsilon(\mathbf{x}, t)$ for $\mathbf{x} \in I$.

All cells are able to change their state. It is important to notice that direct state changes from fluid to gas and vice versa are not possible. Hence, fluid and gas cells are only allowed to transform into interface cells whereas interface cells can be transformed into both gas and fluid cells. A fluid cell is transformed into an interface cell if a direct neighbor is transformed into a gas cell. At the moment of transformation the fluid cell contains a certain amount of fluid mass M which is stored. During further development the interface cell may gain mass from or lose mass to the neighboring cells. These mass currents are calculated and lead to a temporal change of M . If M drops below zero, the interface cell is transformed into a gas cell. It is important to pronounce that mass and density are completely decoupled for interface cells. While the density of the interface cells is given by the pressure boundary conditions and fluid dynamics,

Table I. Cell Types: State Variables and Possible State Transformations

Cell type	f_i, g_i	Fluid fraction ϵ	Gas pressure p^G	Change of state
Fluid F	•	–	–	→ I
Gas G	–	–	•	→ I
Interface I	•	•	•	→ G, → F

•: defined, –: undefined.

M is determined by the mass exchange ΔM with the neighboring fluid and interface cells.

The mass exchange $\Delta M_i(\mathbf{x}, t)$ between an interface cell at lattice site \mathbf{x} and its neighbor in \mathbf{e}_i -direction at $\mathbf{x} + \mathbf{e}_i$ is calculated as:

$$\Delta M_i(\mathbf{x}, t) = \begin{cases} 0, \\ f_i^{\text{out}}(\mathbf{x} + \mathbf{e}_i, t) - f_i^{\text{out}}(\mathbf{x}, t), \\ \frac{1}{2}(\epsilon(\mathbf{x}, t) + \epsilon(\mathbf{x} + \mathbf{e}_i, t))(f_i^{\text{out}}(\mathbf{x} + \mathbf{e}_i, t) - f_i^{\text{out}}(\mathbf{x}, t)), \end{cases}$$

$$\mathbf{x} + \mathbf{e}_i \in \begin{cases} \text{G}, \\ \text{F}, \\ \text{I}, \end{cases} \quad (9)$$

where $\mathbf{e}_i = -\mathbf{e}_i$.

There is no mass transfer between gas and interface cells. The interchange between an interface and a fluid cell should be the same as that of two fluid cells since the cell boundary is completely covered with liquid. In this case, the mass exchange can be directly calculated from the particle distribution functions. The interchange between two interface cells is approximated by assuming that the mass current is weighted by the mean occupied volume fraction. It is crucial to note that mass is explicitly conserved in Equation (9):

$$\Delta M_i(\mathbf{x} + \mathbf{e}_i, t) = -\Delta M_i(\mathbf{x}, t). \quad (10)$$

That is, the mass which a certain cell receives from a neighboring cell is automatically lost there and vice versa. The temporal evolution of the mass content of an interface cell is thus given by

$$M(\mathbf{x}, t + \Delta t) = M(\mathbf{x}, t) + \sum_{i=1}^b \Delta M_i(\mathbf{x}, t). \quad (11)$$

An interface cell is transformed into a gas or fluid cell if $M < 0$ or $M > \rho$, respectively. At the same moment, new interface cells emerge in order to guarantee the continuity of the interface. The initial distribution functions of these new interface cells are extrapolated from the cells in normal direction towards the fluid. Any undershooting or overrun of the fluid fraction of a former interface cell is evenly distributed on the new interface cells to ensure exact mass conservation. The mass redistribution has only impact on M and does not change the density or the distribution functions.

3.2. Boundary Conditions

3.2.1. Boundary Conditions for the Navier–Stokes Equation

The boundary conditions at the interface of a fluid and a gas state that the velocity of both is equal. In addition, the force performed by the gas has to be balanced by the force performed by the fluid. The distribution functions at the interface have to be adapted in such a way that these conditions are fulfilled. After streaming, only distribution functions from fluid and interface cells are defined. Distribution functions arriving from gas cells are not defined within interface cells (see Fig. 3, left).

In the following, a reconstruction procedure for the missing distribution functions is presented where the kinetic nature of the LBM is explicitly exploited. Our approach to fulfill the force boundary conditions is based on a momentum exchange method which was first applied by Ladd^(9,10) to compute the fluid force on a sphere in suspension flow. Mei *et al.*⁽¹¹⁾ have successfully applied a similar approach to calculate forces for problems where curved geometries are involved. The treatment of free interface flows within the momentum exchange method is not known in literature and presented in the following. Our approach is very similar to that of Chen *et al.*⁽¹²⁾ who present a method to fulfill hydrodynamic boundary conditions at curved solid surfaces.

The underlying philosophy of the reconstruction step is that we know the gas pressure and therefrom the force exerted by the gas on the fluid. That is, the boundary conditions are fulfilled if the force exerted by the liquid equals the gas force. The total force is produced by the particles crossing the interface in one time step, i.e., the particle currents from the liquid to the gas and vice versa. Only fluid particles with appropriate velocity, i.e., $\mathbf{n} \cdot \mathbf{e}_i < 0$, will traverse the interface during the advection step.

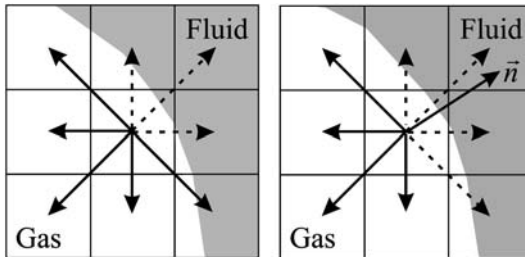


Fig. 3. Missing distribution functions at interface cells after streaming. Left: Undefined distribution functions after streaming (broken lines). Right: Set of distribution functions with $\mathbf{n} \cdot \mathbf{e}_i \geq 0$ (broken lines). The normal \mathbf{n} is determined by a marching cube algorithm [8].

The same is true for particles originating from the gas. In this case, the velocity of the particles must point inwards, $\mathbf{n} \cdot \mathbf{e}_i \geq 0$ (Fig. 3, right).

Thus, the total force \mathbf{F} exerted by the fluid on a surface element $\mathbf{A}(\mathbf{x}) = \mathbf{n} \cdot A(\mathbf{x})$ results from the momentum transported by the particles streaming through this element during one-time step (Fig. 4),

$$F_\alpha = -n_\beta A(\mathbf{x}) \left[\sum_{i, \mathbf{n} \cdot \mathbf{e}_i < 0} f_i^{\text{out}}(\mathbf{x}, t)(e_{i,\alpha} - v_\alpha)(e_{i,\beta} - v_\beta) + \sum_{i, \mathbf{n} \cdot \mathbf{e}_i \geq 0} f_i^{\text{out}}(\mathbf{x} - \mathbf{e}_i, t)(e_{i,\alpha} - v_\alpha)(e_{i,\beta} - v_\beta) \right], \quad (12)$$

where f_i^{out} denotes the particle distribution functions after collision and before advection. In Equation (12), the pure advection term is eliminated by subtracting the interface velocity from the particle velocities. At an interface $b/2$ of the b possible velocity directions point from gas to fluid while the others point from fluid to gas. The first sum contains all known distribution functions coming from the liquid going into the gas. The second part contains all unknown distribution functions coming from the gas and going into the liquid. The unknown incoming distribution functions ($\mathbf{n} \cdot \mathbf{e}_i \geq 0$) have to be chosen in such a way that the boundary conditions are satisfied, i.e., the force \mathbf{F} must balance the gas force.

The symmetry between known and unknown distribution functions, i.e., if f_i is known $f_{\bar{i}}$ is unknown, is essential to fulfill the boundary conditions. We demand force balance for opposite lattice directions. In addition,

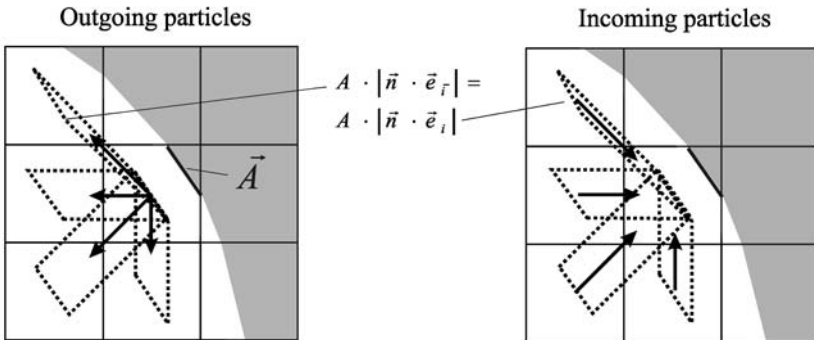


Fig. 4. Particle currents at interface cells. The momentum transferred to the interface area A is proportional to the number of particles which flow through it during one time step (for simplicity $\mathbf{v} = 0$). Left: Outgoing particles. Right: Incoming particles.

we make use of the fact that the forces exerted by the gas are known and are given by the gas pressure and the velocity at the interface. Hence, the missing distribution functions are reconstructed as

$$f_i^{\text{out}}(\mathbf{x} - \mathbf{e}_i, t) = f_i^{\text{eq}}(\rho^G, \mathbf{v}) + f_i^{\text{eq}}(\rho^G, \mathbf{v}) - f_i^{\text{out}}(\mathbf{x}, t), \quad \forall i : \mathbf{n} \cdot \mathbf{e}_i \geq 0 \quad (13)$$

with the gas density $\rho^G(t) = 3p^G(t)$ and the velocity $\mathbf{v} = \mathbf{v}(\mathbf{x}, t)$ of the interface cell.

Inserting Equation (13) in Equation (12) gives:

$$\begin{aligned} F_\alpha/A &= -n_\beta \sum_{i, \mathbf{n} \cdot \mathbf{e}_i < 0} f_i^{\text{out}}(\mathbf{x}, t)(e_{i,\alpha} - v_\alpha)(e_{i,\beta} - v_\beta) \\ &\quad - n_\beta \sum_{i, \mathbf{n} \cdot \mathbf{e}_i \geq 0} \left[f_i^{\text{eq}}(\rho^G, \mathbf{v}) + f_i^{\text{eq}}(\rho^G, \mathbf{v}) - f_i^{\text{out}}(\mathbf{x}, t) \right] (e_{i,\alpha} - v_\alpha)(e_{i,\beta} - v_\beta) \\ &= -n_\beta \sum_{i, \mathbf{n} \cdot \mathbf{e}_i \geq 0} \left[f_i^{\text{eq}}(\rho^G, \mathbf{v}) + f_i^{\text{eq}}(\rho^G, \mathbf{v}) \right] (e_{i,\alpha} - v_\alpha)(e_{i,\beta} - v_\beta) \\ &= -n_\beta \sum_i f_i^{\text{eq}}(\rho^G, \mathbf{v})(e_{i,\alpha} - v_\alpha)(e_{i,\beta} - v_\beta) \\ &= -n_\beta \delta_{\alpha\beta} p^G \\ &= -n_\alpha \cdot p^G \end{aligned} \quad (14)$$

The resulting fluid pressure has the same value as the gas pressure but with the opposite direction $-\mathbf{n}$, i.e., the physical boundary condition is fulfilled. Below, it is shown that the reconstruction algorithm works very well. Nevertheless, the effective precision is not yet rigorously verified.

It is important to note that not only the missing distribution functions are reconstructed but all distribution functions with $\mathbf{e}_i \cdot \mathbf{n} \geq 0$ (see Fig. 3, right). At first glance, part of the information seems to be disregarded since some of the distribution functions coming from neighboring interface cells are not taken into account. In order to resolve this apparent contradiction it is instructive to remind that this seemingly discrepancy originally results from the treatment of the interface cells. They are more or less treated as fluid cells with a full set of distribution functions defining the fluid. This brings some kind of asymmetry into the interface treatment since the number of unknown incoming distribution functions is generally smaller than the number of the known. The above procedure restores symmetry between gas and fluid since interface cells

are sometimes treated as gas or as fluid depending on the actual interface orientation. Generally, half of the set of the distribution functions is reconstructed.

After completion of the whole set of distribution functions, the new density ρ and velocity \mathbf{v} can be calculated. The outgoing distribution functions are calculated as

$$f_i^{\text{out}}(\mathbf{x}, t) = f_i^{\text{in}}(\mathbf{x}, t) - \frac{1}{\tau} \left(f_i^{\text{in}}(\mathbf{x}, t) - f_i^{\text{eq}}(\rho, \mathbf{v}) \right) + \epsilon_i(\mathbf{x}, t) w_i \rho(t) \mathbf{e}_i \cdot \mathbf{g}, \quad \forall \mathbf{x} \in I \quad (15)$$

Similar to the volume of fluid method gravity is weighted in Equation (15) by the volume fraction of the cell. This is the same procedure as in refs. 13 and 14.

The effect of the surface tension is treated as a local modification of the gas pressure p^G

$$p^G(t) = \frac{1}{3} \rho^G(t) - 2\kappa(t)\sigma - \Pi, \quad (16)$$

where ρ^G is the gas density and κ and σ denote the curvature and the surface energy, respectively. The disjoining pressure Π comprises the forces which stabilize the foam structure. Π is a function of the distance to the nearest neighboring interface d_{int} :

$$\Pi(d_{\text{int}}) = \begin{cases} c_{\Pi} |d_{\text{range}} - d_{\text{int}}|, & d_{\text{int}} < d_{\text{range}}, \\ 0, & d_{\text{int}} \geq d_{\text{range}}, \end{cases} \quad (17)$$

where the magnitude and the range of the disjoining pressure are determined by the two phenomenological parameters c_{Π} and d_{range} .

We use two different methods to determine the curvature. In 2D a template sphere method⁽¹⁵⁾ is applied which uses an extended neighborhood of 25 cells to estimate the curvature. In 3D a marching cube algorithm is used which leads to a representation of the interface by triangles. The curvature κ belonging to a triangle is estimated by $\kappa = \frac{1}{2}(\delta A / \delta V)$ where δA denotes the alteration of the triangle area when its vertices are infinitesimally shifted in normal direction. The respective volume change is denoted by δV . The curvature of an interface cell is estimated by the mean curvature of the triangles belonging to it.

3.2.2. Boundary Conditions for the Diffusion–Convection Equation

The macroscopic boundary condition for the gas diffusion problem reads

$$c(\mathbf{x}) = c^G \underbrace{\quad}_{\text{Sieverts' law}} S \sqrt{p^G}, \quad \mathbf{x} \in I, \quad (18)$$

where Sieverts' law relates the equilibrium gas concentration c^G to the gas pressure p^G . Sieverts' law is a variant of the well-known Henry's law and is valid if the gas does not consist of single atoms but molecules from two atoms like, e.g., H_2 . S denotes Sieverts' constant which is a material dependent parameter. Translating this boundary condition into the lattice Boltzmann picture we have to demand that the incoming particle currents at interface cells (interface cells have at least one undefined g_i after streaming) add to the interface concentration,

$$\sum_i g_i^{\text{in}}(\mathbf{x}, t) = c^G. \quad (19)$$

The last equation can be fulfilled by demanding the distribution functions with $\mathbf{n} \cdot \mathbf{e}_i \geq 0$ to obey the following relation:

$$g_i^{\text{in}}(\mathbf{x}, t) = \begin{cases} g_i^{\text{eq}}(c^G, \mathbf{v}) + g_i^{\text{eq}}(c^G, \mathbf{v}) - g_i^{\text{in}}(\mathbf{x}, t), & \text{if } g_i^{\text{in}}(\mathbf{x}, t) \text{ defined,} \\ g_i^{\text{eq}}(c^G, \mathbf{v}), & \text{if } g_i^{\text{in}}(\mathbf{x}, t) \text{ not defined.} \end{cases} \quad (20)$$

Gas cells surrounded by interface cells built connected and closed areas of cells which represent the bubbles. All cells belonging to one bubble share the same information of the bubble properties, namely the interior bubble pressure, the bubble volume and the contained amount of hydrogen gas. Volume and amount of substance of the bubbles are changed by the liquid flow and diffusion across the interface. The bubble pressure results from the bubble volume and bubble gas content via the ideal gas equation.

4. VERIFICATION

In the following, verification tests are presented which concern the fluid dynamic problem, i.e., advection of the interface and the boundary conditions.

4.1. Advection

As a simple test for the advection algorithm, a bubble (2D) and a drop (3D) are moved with constant velocity \mathbf{v} at different grid resolution, i.e., different bubble and drop diameters $D = 10, 20, 40, 80$. This test completely decouples advection from the free surface problem since the distribution functions are constant, i.e., $f_i = f_i^{\text{eq}}(\mathbf{v}, \rho) = \text{const.} \quad \forall i, \mathbf{x} \in \{F, I\}$. Consequently, all errors can be exclusively traced back to the advection algorithm. Figure 5 shows the 2D-bubble and 3D-drop for different

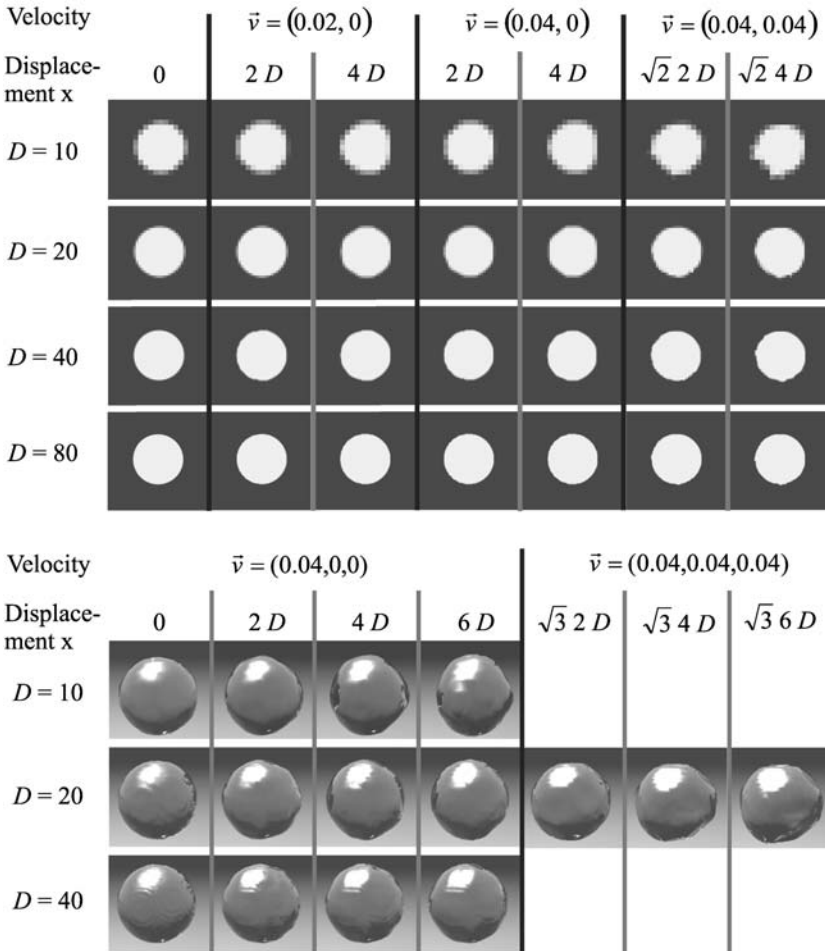


Fig. 5. Advection test. A bubble (2D, top) and a drop (3D, bottom) are advected with constant velocity and different resolution along the lattice coordinates and the diagonal direction.

velocities and directions after different translation distances. Generally, the overall shape of the drop is maintained but with increasing distance deformations get visible. These deformations are anisotropic and minimal if advection is along the lattice axes and maximal in diagonal direction.

The accuracy of the advection of the 2D-bubble center can be inferred from Table II giving the relative errors err of the position of the bubble centers \mathbf{R}_c for different resolutions as a function of the covered distance \mathbf{vt} :

$$err(\mathbf{vt}) = \frac{\|\mathbf{R}_c(t) - \mathbf{vt} - \mathbf{R}_c(0)\|}{\|\mathbf{vt}\|}. \tag{21}$$

The convergence rates are about second order. The movement along the diagonal with $\mathbf{v} = (0.04, 0.04)$ results in relative errors which are a factor 2 – 10 larger. In this case the convergence rates are between first and second order. In 3D, the relative discrepancies of the drop center from the expected value are in the range of 10^{-2} for $D=10$ and 10^{-3} for $D=40$. The deformations are analogous to that in two dimensions.

In the following, the advection algorithm is compared with the recoloring LB algorithm applied by Ginzburg and Steiner.⁽¹⁴⁾ For that purpose, a spherical bubble is placed on lattices with different resolutions $2^n \times 2^n$, where $n = 5, 6, 7$. Initially, the bubble center is given by $\mathbf{R}_c(0) = (2^{n-1}, 2^{n-1})$. The bubble radius is $R = 7 \times 2^{n-5}$. The error norm $\|err\|$ is calculated according to the following relation:⁽¹⁴⁾

$$\|err\| = \frac{2^{5-n}}{2} \sum_{\alpha} \sum_{k=1}^7 \|R_{\alpha}(t(k)) - R_{c,\alpha} - v_{\alpha}t\| \tag{22}$$

Table II. Advection Test with Velocity $\mathbf{v} = (0.04, 0)$

Diameter $D = 10 \times 2^n$	$n = 0$ $D = 10$	$n = 1$ $D = 20$	$n = 2$ $D = 40$	$n = 3$ $D = 80$
$err(2D)$	4.48×10^{-3}	9.25×10^{-4}	1.29×10^{-4}	3.5×10^{-5}
$\sqrt{\frac{err(2D,n)}{err(2D,n+1)}}$		2.2	2.67	1.92
$err(4D)$	4.23×10^{-3}	1.1×10^{-3}	1.69×10^{-4}	3.96×10^{-5}
$\sqrt{\frac{err(4D,n)}{err(4D,n+1)}}$		1.96	2.55	2.06

The relative error err of the position of the bubble center is given for different distances and resolutions n .

Table III. Error Norm $\|\text{err}\|$ of a 2D-bubble Advected by a Uniform Velocity Field [15]

(v_x, v_y)	32×32	64×64	128×128
(0.10, 0.00)	0.0267	0.0053	0.0012
(0.10, 0.10)	0.0771	0.0406	0.0104
(0.05, 0.10)	0.0608	0.0243	0.0064

with $t = 10 \cdot k \cdot 2^{n-5}$ and $k = 1, \dots, 7$. The error for our algorithm (Table III) remains significantly below that reported by Ginzburg and Steiner.^(13,14) However, a strict comparison is not possible, since our analysis is only two-dimensional.

4.2. Boundary Conditions

Two examples, a capillary wave in 2D and a rising bubble in 3D, are employed to verify the boundary conditions. Verification of the boundary conditions can not be carried out without advection. Thus, inaccuracies are always the result of a superposition of inaccuracies within the advection algorithm and the treatment of the free boundary. Nevertheless, the last paragraph has shown that advection works rather well. Therefore, strong deviations from analytical results are expected to be mostly due to inaccuracies in the boundary conditions.

4.2.1. Capillary Wave

A small sinusoidal disturbance of a fluid–gas interface is considered. Such a disturbance is oscillating around its mean value due to capillary forces. It is eventually damped down by internal friction. If damping is small there are analytical solutions for the long wavelength limit:⁽¹⁶⁾

$$y(t) = y(0) + A_0 \cos(\omega t) \cdot e^{-\kappa t} \quad (23)$$

with y as interface position in y -direction, A_0 as initial amplitude. The frequency ω and the damping factor κ are given by

$$\omega = \sqrt{k^3 \sigma}, \quad \kappa = 2k^2 \nu, \quad (24)$$

where $k = 2\pi/\lambda$ denotes the wave number and λ the wavelength.

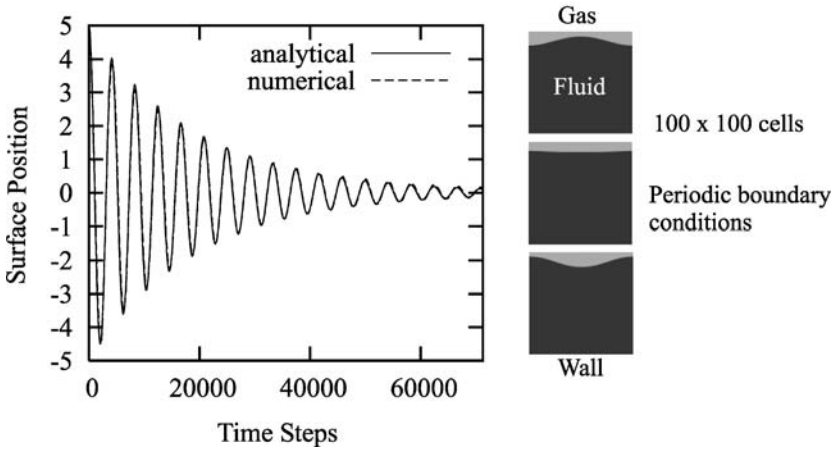


Fig. 6. Capillary wave. Oscillation of a point at the gas–fluid interface driven by surface tension (lattice: 100×100 , $g = 0$, $\sigma = 0.01$, $\tau = 0.52$). Full line: Numerical result, broken line: Analytical result with the frequency reduced by 4%.

Figure 6 shows the oscillation of a capillary wave. The deviation of the oscillation frequency from the analytical value is about 4% for the 100×100 lattice. The error decreases linearly with increasing resolution. The damping factor κ is perfectly reproduced. Similar verification experiments for alternative multiphase LB models as in ref. 17 show the same or even larger deviations from the theoretical predictions. The shape of the sinusoidal wave is maintained during many oscillations, even when the amplitude falls below the cell size.

4.2.2. Rising Bubble

A single gas bubble within an infinite fluid is considered. The bubble rises due to gravity and eventually reaches a stationary velocity v where the drag force balances buoyancy. If the deformation of the bubble is negligible, the stationary rising velocity follows from force balance between the dragging force given by Stokes’ law and buoyancy,⁽¹⁶⁾

$$v = \frac{gR^2}{3\nu}, \tag{25}$$

where R is the bubble radius, ν the kinematic viscosity and g the gravity constant.

A system with $100 \times 100 \times 160$ cells is considered. In addition, periodic boundary conditions in x - and y -direction are applied. The following

parameters are used: $R = 8$, $\sigma = 2 \times 10^{-2}$, $\tau = 1.46$, $g = 10^{-4}$. After 10000 time steps and a distance of 60 lattice units the numerical velocity is about 0.00653 whereas the theoretical velocity is 0.00667. The relative difference is about 2%. Other parameter combinations and bubble radii lead to similar results. If the bubble radius is $R = 4$ and $\tau = 0.74$ the bubble velocity after 10.000 time steps is 0.006714. In this case the relative error between theoretical and numerical result reduces to 0.7%. We suppose that the larger part of the difference between the theoretical and the numerical velocity can be traced back to the finite system size, i.e., Equation (25) is not the exact solution for a finite system.

5. APPLICATION

The applications for our LBM for free surface flow are foaming processes, especially foaming of metals. Global phenomena like drainage, topological rearrangements, avalanche-like rearrangements and avalanche-like coalescence processes emerge from our model only without further assumptions. Figure 7 shows the growth and the subsequent aging of a foam. Other results of 2D-modeling of foaming processes including gas diffusion can be found in refs. 2 and 18.

In 3D, diffusion is not yet included. Nevertheless, foaming can be modeled by assuming that the bubble gas content increases by a certain amount in each time step which is proportional to the respective bubble interface area. An example is depicted in Fig. 8. A large number of bubbles starts growing within the fluid. The disjoining pressure delays bubble coalescence but does not completely prevent it. Consequently, the number

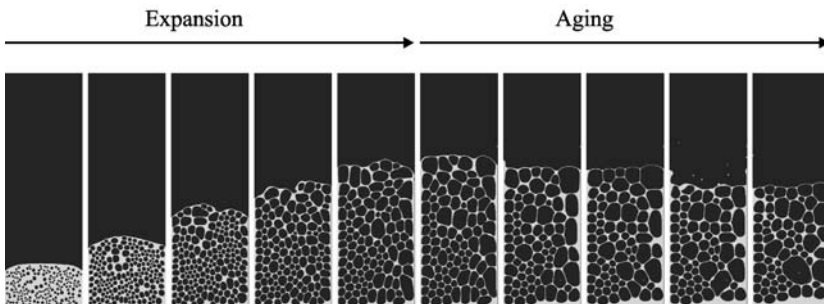


Fig. 7. Foam expansion and subsequent aging. Gravity leads to a pronounced drainage zone at the bottom. ($\nu = 0.42$, $\sigma = 0.01$, $D = 0.075$, $g = 3 \times 10^{-5}$, $Q = 5 \times 10^{-5}$ as long as the number of time steps is smaller than 50000, $S = 5 \times 10^{-4}$, $c_{\Pi} = 3 \times 10^{-3}$, total number of time steps: 100000, lattice: 300×900 .)

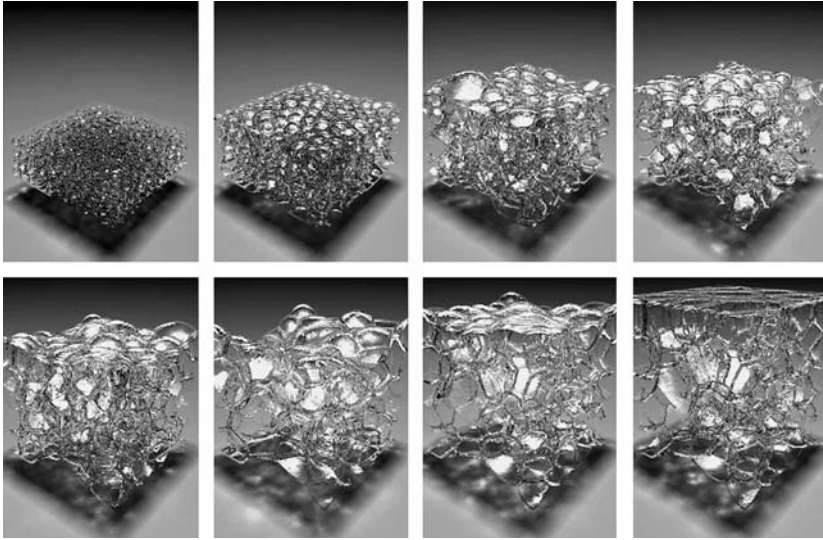


Fig. 8. 3D-Foam. Initial number of bubbles is 1000, final number is 57. The bubbles grow and coalescence occurs. The disjoining pressure Π stabilizes the foam and eventually a polygonal structure develops. (System size: $120 \times 120 \times 140$, $\tau = 0.65$, $g = 0$, $\sigma = 0.01$, $c_{\Pi} = 0.006$, total number of time steps: 73000.)

of bubbles decreases with increasing gas volume. At the end, a polygonal foam structure has developed.

6. CONCLUSIONS

In this work we propose a LB scheme to deal with free surface flows. This method can be regarded as a surface capturing method. The liquid is confined by a completely closed layer of interface cells characterized by an additional state variable, the volume fraction of fluid. The movement of the surface and the fulfillment of the pressure boundary conditions is modeled by using the mass and momentum fluxes across the interface. The calculation of the fluxes is based on the particle distribution functions. This current based procedure allows control of the hydrodynamic fluxes across the interface without explicit calculation of gradient information. A similar procedure is applied to fulfill the diffusion boundary condition.

The proposed scheme is robust, stable, and easy to implement. Simple verification tests demonstrate the correctness of the algorithms. It is successfully applied to the simulation of foam evolution problems.

ACKNOWLEDGMENTS

The work was supported by the Deutsche Forschungsgemeinschaft DFG (SPP 1075) and KONWIHR.

REFERENCES

1. C. Körner, M. Thies, M. Arnold, and R. F. Singer, The physics of foaming: structure formation and stability, in *Handbook of Cellular Metals*, H. P. Degischer and B. Kriszt, eds. (Wiley-VCH, 2002), pp. 33–42.
2. C. Körner, M. Thies, and R. F. Singer, Modeling of metal foaming with lattice Boltzmann automata, *Adv. Eng. Mater.* **4**:765–769 (2002).
3. C. Körner, M. Hirschmann, M. Lamm, and R. F. Singer, Magnesium integral foams, in *Cellular Metals. Manufacture, Properties, Applications*, J. Banhart et al. eds. (Verlag MIT Publishing, Berlin, 2003), pp. 209–214.
4. X. He and L.-S. Luo, Theory of the lattice Boltzmann method: from the Boltzmann equation to the lattice Boltzmann equation, *Phys. Rev. E*, **56**:6811–6817 (1997).
5. P. Bhatnagar, E. Gross, and M. Krook, A model for collision process in gases I: small amplitude processes in charged and neutral one-component system, *Phys. Rev. E* **50**:511–525 (1954).
6. Y. H. Qian, D. d’Humières, and P. Lallemand, Lattice BGK models for Navier-Stokes equation, *Europhys. Lett.* **17**:479–484 (1992).
7. D. Wolf-Gladow, A Lattice Boltzmann equation for diffusion, *J. Stat. Phys.* **79**:1023–1032 (1995).
8. W. Lorenzen and H. Cline, Marching cubes: A high resolution 3D surface reconstruction algorithm, *Comput. Graph.* **21**:163–169 (1987).
9. A. Ladd, Numerical simulations of particulate suspensions via a discretized Boltzmann equation. Part 1, *J. Fluid Mech.* **271**:285 (1994).
10. A. Ladd, Numerical simulations of particulate suspensions via a discretized Boltzmann equation. Part 2, *J. Fluid Mech.* **271**:311 (1994).
11. R. Mei, D. Yu, W. Shyy, and L.-S. Luo, Force evaluation in the lattice Boltzmann method involving curved geometry, *Phys. Rev. E* **65**:041203/1–14 (2002).
12. H. Chen, C. Teixeira, and K. Molvig, Realization of fluid boundary conditions via discrete Boltzmann dynamics, *Int. J. Mod. Phys.* **9**:1281–1992 (1998).
13. I. Ginzburg and K. Steiner, A free-surface lattice Boltzmann method for modelling the filling of expanding cavities by Bingham fluids, *Phil. Trans. R. Soc. Lond. A* **360**:453–466 (2002).
14. I. Ginzburg and K. Steiner, Lattice Boltzmann model for free-surface flow and its application to filling process in casting, *J. Comput. Phys.* **185**:61–99 (2003).
15. M. Thies, Lattice Boltzmann modeling with free surfaces applied to in-situ gas generated foam formation, PhD-Thesis, University of Erlangen-Nürnberg (2005).
16. L. D. Landau and E. M. Lifschitz, *Hydrodynamik* (Akademie-Verlag, Berlin 1974).
17. R. Zhang, X. He, and S. Chen, Interface and surface tension in incompressible lattice Boltzmann multiphase model, *Comput. Phys. Commun.* **129**:121–130 (2000).
18. C. Körner, M. Thies, M. Arnold, and R. F. Singer, Modeling of metal foaming by in-situ gas formation, in *Cellular Metals. Manufacture, Properties, Applications*, J. Banhart et al. eds. (Verlag MIT Publishing, Bremen, 2001), pp. 93–98.